Absorption of solar radiation by noctilucent clouds in a changing climate

Franz-Josef Lübken[1], Gerd Baumgarten[1], Mykhaylo Grygalashvyly[1], and Ashique Vellalassery[1]

[1]Leibniz Institute of Atmospheric Physics, Schloss-Str.6, 18225 Kühlungsborn, Germany, www.iap-kborn.de

Key Points:

- Noctilucent clouds (NLC) are ice clouds in the summer mesopause region at middle and polar latitudes.
- The future concentration of water vapor at NLC heights will increase and more and larger ice particles are expected.
- Larger ice particles will lead to an enhanced absorption of solar radiation.

Corresponding author: Franz-Josef Lübken, `luebken@iap-kborn.de`

Abstract

The future increase of methane concentration leads to a raise in water vapor abundance in the middle atmosphere. This will enhance the brightness of noctilucent clouds (NLC). We use an atmospheric background model and a microphysical model to study the associated absorption of solar radiation in the period 1950 to 2100. At 69°N mean absorptions at λ=126 nm will increase from ∼3% to ∼7% from 1950 to 2100, respectively. Locally, the absorption can increase to ∼30% in the year 2100. In the visible we find an increase from 0.0030% (1950) to 0,020% (2100), i.e., by a factor of ∼7, and local maxima up to 0.35% in 2100. The results are similar for polar latitudes (79°N) but are smaller at middle latitudes (58°N). Future mean absorptions are comparable to solar cycle variations, but much larger locally. The ice mass bound in NLC increases from 677 to 1871 tons in 1950 and 2100.

Plain Language Summary

Noctilucent clouds (NLC) consist of water ice particles and appear in the summer season in the upper mesosphere at high/middle latitudes where temperatures are very low. Methane is photochemically converted to water vapor in the middle atmosphere. Therefore, the future increase of methane concentration will lead to a raise in water vapor, and to an enhancement of NLC occurrence and brightness. We apply an atmospheric background model and a microphysical ice particle model to study the associated absorption of solar radiation. At 69°N mean absorptions in the UV will increase from ∼3% to ∼7% from 1950 to 2100, respectively. Locally, the absorption can increase to ∼30% in 2100. In the visible (λ=532 nm) the corresponding numbers are 0.0030% (1950) to 0,020% (2100), i. e., an increase by a factor of ∼7, and local maxima up to 0.35% in 2100. Mean absorptions are comparable to variations throughout a solar cycle, but may locally be much larger. Effects on the photochemistry are therefore expected. The total amount of ice mass bound in NLC also increases with time, namely from 677 tons in 1950 to 1871 tons in 2100. NLC will be easier to observe by naked eye, i.e., they will be more frequent and brighter.

1 Introduction

Noctilucent clouds (NLC) consist of water ice particles and appear in the summer season in the upper mesosphere at high and middle latitudes where temperatures are very low (e. g. Gadsden & Schröder, 1989, and references therein). There is a long standing scientific dispute, if or not NLC are indicators of climate change, where an unequivocal proof by observations is still pending (see, for example, Thomas, 2003; Pertsev et al., 2014; Russell III et al., 2015; Berger & Lübken, 2015; Fiedler et al., 2017). Results on the future development of NLC have recently been published by Yu et al. (2023), but a 0-d model was applied for NLC and no extinctions were calculated. It is generally assumed that the optical thickness of these clouds is on the order of 10^{-4} or less, i. e., too small to cause a significant extinction of solar radiation (e.g., Kokhanovsky, 2005). It has been shown in previous studies that the main reason for an increase of extinction by NLC is given by an increase of water vapor which is expected to grow in the middle atmosphere due to enhanced emissions of methane (in the troposphere) which is photochemically converted to water vapor in the middle atmosphere. In this paper we study the extinction of solar radiation by NLC at various wavelengths in a future climate scenario with increasing methane. We use the atmospheric background model LIMA (Leibniz Institute Middle Atmosphere Model) and a microphysical model of ice particle formation called MIMAS (Mesospheric Ice Microphysics And tranSport model). Various results on the historical NLC development based on LIMA/MIMAS are described in Lübken et al. (2021), hereafter refered to as LBB21, and references therein.

2 Model

For the background atmosphere we use the global model LIMA (0–150 km) which is nudged to the real atmosphere at lower heights. More details are described elsewhere (Berger & von Zahn, 2002; Berger, 2008; Berger & Lübken, 2011). For this study we use background conditions from a representative year (1982) for all years, i. e., the dynamical forcing of the upper mesosphere/lower thermosphere is kept constant for all years. In MIMAS the formation of ice particles is determined by investigating the fate of a total of 40 million dust/ice particles. Note that we use the full size distribution of ice particles to calculate extinction coefficients whereas assuming a single (mean) radius and a theoretical size distribution leads to significant uncertainties.
In MIMAS the interaction of ice particles with background water vapor is considered, including freeze drying. In this study we consider in increase of methane only (leading to an increase in water vapour as described in LBB21), i. e., keeping temperatures and dynamics constant (note that changing H_2O causes a very small temperature change which can be neglected in this context). We have shown in previous papers that the increase of optical parameters such as brightness and extinction is nearly entirely given by an increase of H_2O, whereas a decrease of temperatures (caused by an increase of carbon dioxide) plays a minor role (see, for example, Fig. 3 in Lübken et al., 2018). In previous studies we have presented various comparisons of results from LIMA and MIMAS with ground based and satellite borne observations and found excellent agreement (see, for example Schmidt et al., 2018; Lübken et al., 2021; Vellalassery et al., 2023, and references therein).
Fig. 1 In Figure 1 we show the temporal behaviour of methane concentration in the troposphere used in MIMAS. The expected future development is based on IPCC AR4. More specifically, we use the RCP8.5 scenario as descibred in Riahi et al. (2011) which turned out to be realistic so far.

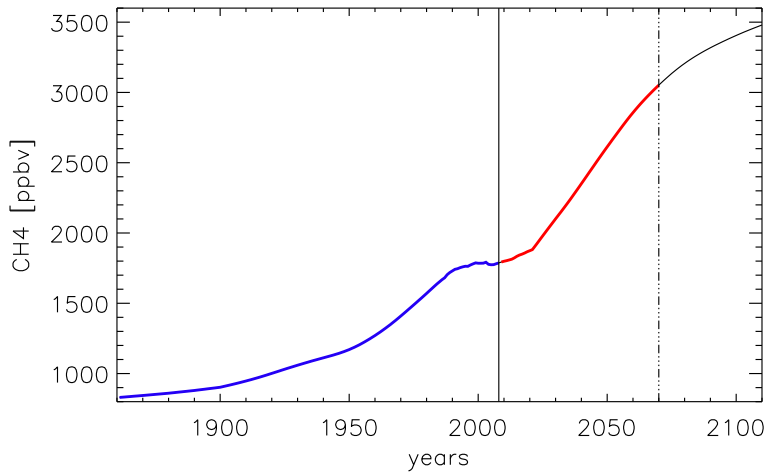

Figure 1. Concentrations of methane in the troposphere (blue) as used in LIMA/MIMAS, including future projections taken from IPCC (red)

For computational reasons we use LIMA/MIMAS model results from selected years in the period 1950 to 2100. Furthermore, we consider the core of the NLC season only, namely the month of July. As in LBB21, we study three latitude bands, namely 58±3°N, 69±3°N, and 78±3°N, respectively. In total there are 89,280 columns per year in each

latitude band, since there are 6 latitudes, 120 longitudes, 31 days, and 4 timesteps per day. Note that the ice layer and related optical parameters may vary substantially from column to column. We have considered the large solar zenith angles at high latitudes in summer (we have used χ=80° as a representative value) by increasing the optical depths and related parameters by a factor of 5.76, i. e., $1/\cos\chi$ approximating the Chapman function. Furthermore, we have increased all radii by a factor of 1.35, following the results presented in Schmidt et al. (2018).

The extinction coefficient ('cross section') $\sigma(r,\lambda)$ (units: m^2) is a function of particle radius r and wavelength λ. It is needed to calculate the optical depth $d\tau$ for a given wavelength λ traversing a layer at height z with a geometrical thickness dz:

$$d\tau(z,r,\lambda) = \sigma(r,\lambda) \cdot dz \cdot dN(z,r,dr) \quad [/] \tag{1}$$

where $dN(z,r,dr)$ is the number density of particles at height z with radius between r and $r+dr$. The total optical depth $\tau(\lambda)$ is determined by integrating over all radii. The amount of solar light with wavelength λ passing the layer (relative to the incoming intensity) is $\exp(-\tau)$, and the relative attenuation is $a = 100 \cdot (1 - e^{-\tau})$ (in %). For a ground-based lidar the backscatter coefficient β determines the amount of laser light being backscattered. In MIMAS, backscatter coefficients and optical depths are determined for every box, i. e., at all altitude layers at all latitudes/longitudes and time steps. The effect of several boxes is given by summation over all τ.

In Figure 2 we show extinction coefficients as a function of wavelengths for monodispers particles with given radii. In a significant part of the spectrum in the visible and infrared (i. e., between roughly 200-1000 nm) the extinction coefficient varies as λ^{-4} for a given radius, and approximately as r^6 for a given wavelength. This implies that i) the size of the NLC particles is crucial for the total extinction, and ii) the absorption of solar radiation generally decreases rapidly with increasing wavelength. This is no longer true for wavelengths larger than ∼1000-2000 nm, and for radii smaller than ∼200 nm. Mie calculations were performed assuming mono-dispers spherical ice particles applying the wavelength dependent refractive index values from Warren and Brandt (2008). The resonances with a major peak at ∼3000 nm are due to vibrational excitation of OH.

Fig. 2

3 Results

In Figure 3 the relative occurrence frequencies of maximum backscatter coefficients (β_{max}) from LIMA/MIMAS are presented for a given year (2000) considering all columns in the latitude band 69±3°N. Observational results of β_{max} from the ALOMAR Rayleigh-Mie-Raman (RMR) lidar at 69°N for the years 1997-2020 are shown for comparison (both for the month of July only). A description of the NLC data set obtained from this lidar is presented in Fiedler et al. (2017). Note, that lidar data were averaged over 15 minutes which elimantes very bright NLC. The idea is to characterize the variability of NLC brightness (expressed as β_{max}) from spatial (LIMA/MIMAS) and temporal (ALOMAR) coverage. As can be seen from Figure 3 the relative distribution of β_{max}-values from observations and from the model are very similar which supports the idea that particle size and number density distributions in LIMA/MIMAS are rather realistic, which is then also true for extinction coefficients and attenuations.

Fig. 3

In Figure 4 we present a frequency distribution of attenuations from various years at 69±3°N for a wavelength of λ=200 nm where we have considered boxes only where radii are larger than 2 nm to avoid mixture with dust particles. We have chosen 200 nm since this allows a fairly easy extrapolation to larger wavelengths and the extinction is similar to the maximum around 3000 nm (see Figure 2). From Figure 4 we can identify how often (i. e., in how many columns) a given attenuation appears in a given year, relative to the total number of columns (=89,280). For example, in 2080 and λ=200 nm

Fig. 4

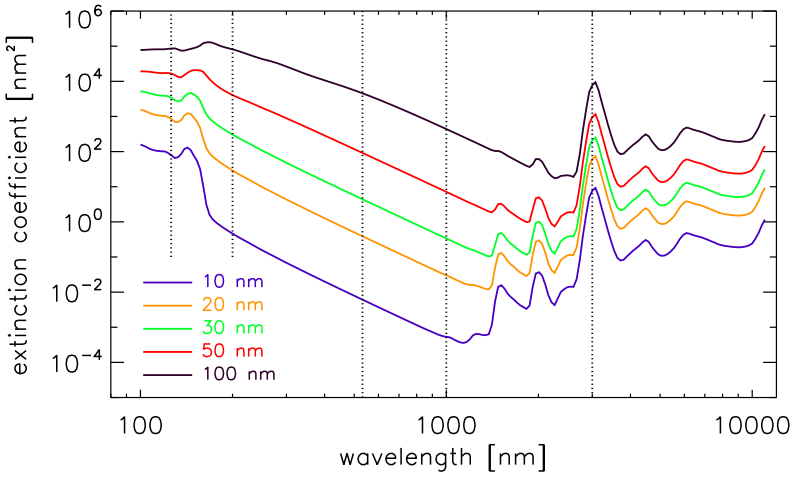

Figure 2. Extinction coefficients as a function of wavelength for (mono-dispers) particle radii as given in the insert (in nm, various colors). The vertical lines mark wavelengths where we have calculated extinctions by the NLC layer.

an attenuation of 2% appears in ∼6% of all columns. Or, the chance to have attenuations of 3% (at λ=200 nm) increases by a factor of roughly 300 from 2000 to 2040. As expected, the distributions shown in Figure 4 drop off less rapidly for future years, i. e., larger attenuations appear more frequently. Note that nearly all columns are filled with ice particles which is consistent with the observation that PMSE (polar mesosphere summer echoes) are present at polar and arctic latitudes in summer nearly all the time (Latteck et al., 2021). Note that PMSE are much less sensitive to ice particle radii compared to NLC. If we limit the occurrence frequency to larger than 1%, the maximum attenuations are roughly 2%, 2.7%, and 4.2% in 2000, 2040, and 2080, respectively. In the visible (λ=500 nm, for example) these values decrease by a factor of roughly $(500/200)^4$=39. For comparison, we also show in Figure 4 the frequency distribution for λ=126 nm in the year 2080, again for 69±3°N. As expected, the distribution extends to much larger attenuations compared to λ=200 nm because the extinction coefficient is larger (see Figure 2).

Fig. 5

In Figure 5 the long term evolution of mean optical thickness and attenuation is shown for λ=126 nm at 69±3°N. The values are determined as follows: for a given year, extinction coefficients $\tau_{i,j,k}$ are available at all i_{max}=124 times steps, j_{max}=6 latitudes, and k_{max}=120 longitudes. First, the mean extinction coefficient $\overline{\tau_i}$ at each time step i is determined, averaging over all latitudes/longitudes but only where NLC are present. Then the mean over all time steps $\overline{\tau_i}$ in a given year is calculated, as well as the standard deviation of the mean and the maximum and minimum values. Furthermore, the maximum of all values in a given year $\tau_{i,j,k}$ is shown, called 'grand maximum'. As can be seen from Figure 5, mean absorptions at λ=126 nm increase from ∼3% to ∼7% from 1950 to 2100, respectively. The mean variability is on the order of a factor of two. Locally, the absorption can increase up to 30% in the year 2100. In the visible (532 nm, not shown) mean attenuations increase from 0.0030% (1950) to 0.020% (2100), i. e., by a factor of ∼7. Locally, maximum values can reach up to 0.35% in 2100.

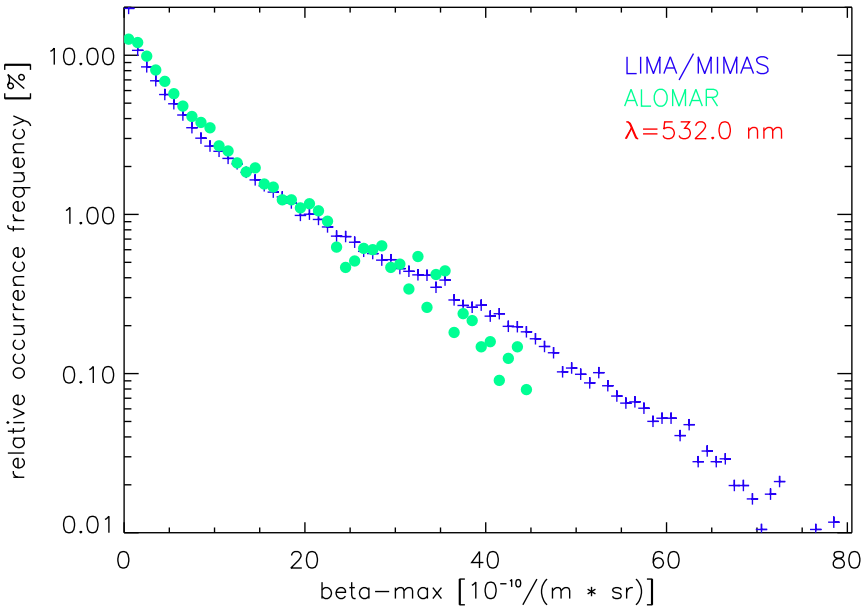

Figure 3. Relative frequency of occurrence (in %) of i) maximum backscatter values (β_{max}, blue crosses) from LIMA/MIMAS in all columns in a given year (2000) in July in the latitude band 69±3°N, and ii) β_{max}-values from the ALOMAR RMR lidar at 69°N during 1-31 July from the years 1997 to 2020 (green dots). Both data sets are for a wavelength of 532 nm.

4 Discussion and Conclusion

We have also studied future extinctions etc. at other latitudes and find similar results (compared to 69±3°N) at 78±3°N, but significantly smaller values at 58±3°N (not shown). The total amount of ice mass bound in NLC also increases with time, namely from 677 tons in 1950 to 1259 and 1871 tons in 2050 and 2100, respectively, where the largest fraction (typically 80-90%) stems from north of 60°N. Generally speaking, the ice mass increases with the concentration of methane, but the correlation is not linear. The ice water content, i. e., the ice mass in a given column, increases correspondingly.

Note that the relative increase of extinction and attenuation with time (see Figure 5 for λ=126 nm) is significantly stronger at larger wavelengths (λ=532 nm, for example) where the extinction is roughly proportional to r^6, whereas the dependence on radius is weaker at 126 nm because the Rayleigh scattering condition $\lambda/2\pi r \gg 1$ is no longer valid. We have checked the results for consistency. For example: the variation of ice mass ($\sim r^3$) and attenuation ($\sim r^6$) are consistent, since (for the years 2100 and 1950) we have (1871 tons/677 tons)$^{1/3}$=1.40 and (for λ=532 nm) we get (0.02056 %/0.00301 %)$^{1/6}$=1.38, which are surprisingly similar when we consider that we have ignored various factors complicating such a comparison.

In order to judge the importance of the solar radiation absorption by NLC we compare with the variability due to the solar cycle, all of which vary substantially with wavelengths. For example, in the visible the solar cycle variation is roughly 0.1% (see, for example, Figure 3 in Gray et al., 2010). We have repeated the trend calculations shown

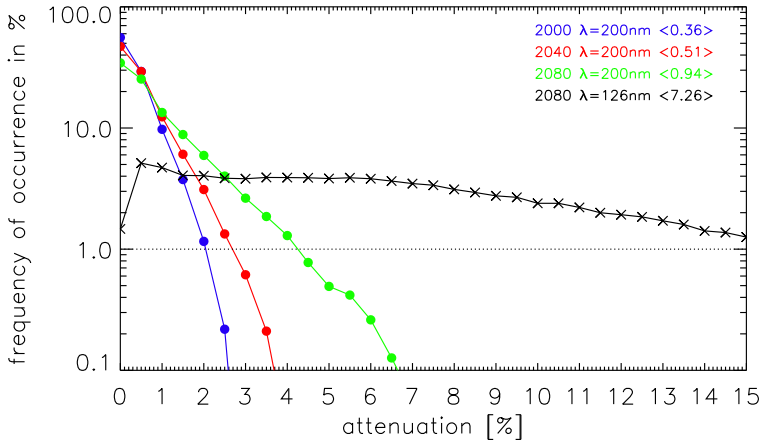

Figure 4. The relative occurrence frequency of attenuations at 69±3°N from various years (see inlet) for a wavelength of λ=200 nm (dots) and λ=126 nm (crosses). The inlet also lists the mean attenuations (<...>) in %.

in Figure 5 for λ=532 nm and find for the year 2100 mean absorptions of 0.02% and (grand) maximum absorptions of $\sim$ 0.35%. The latter implies that in certain areas the maximum absorption by NLC in the visible as expected for 2100 is significantly larger compared to the variation throughout a solar cycle. In the UV (λ=126 nm) the variations are several tens percent, both during a solar cycle and for the maximum absorption by NLC (see Figure 5).

The absorption of solar radiation by NLC will presumable affect photochemical processes at lower heights, in particular those related to odd oxygen. We realize that most of the involved reaction mechanisms are non-linear which means that a sophisticated analysis is required to make quantitative predictions. The same applies for positive feedback mechanisms, which are currently ignored: the absorption of solar UV radiation leads to less dissociation and higher concentrations of water vapor, which leads to more and larger ice particles, which in turn leads to more absorption of solar radiation.

Last but not least, for ground based visible observers at middle latitudes, the conditions to observe NLC become more favorable in the future, i. e., the occurrence frequency and the brightness of NLC will increase substantially.

Acknowledgments

We thank Jens Fieder for providing an update of the lidar data from ALOMAR. The Mie calculations were performed using information from http://atol.ucsd.edu/scatlib/index.htm. This paper was supported by the TIMA project (grant no. 01LG1902A) of the BMBF research initiative ROMIC.

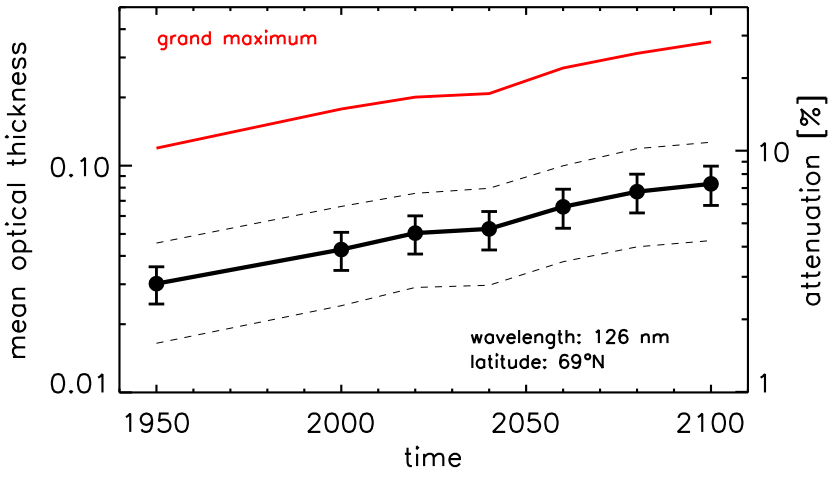

Figure 5. For each selected year the mean extinction coefficients (left axis) and attenuations (right axis) are shown at 69±3°N. First, we average the extinction coefficients from all columns (only where NLC are present) at a given time step. Then we take the extinction coefficients from all time steps and determine the mean (dots), standard deviation (bars), and the maximum and minimum values (dashed lines). Furthermore, the maximum extinction coefficient from all columns (before averaging) is shown (red line, 'grand maximum'). See text for more details.

Open Research

The datasets presented in the 5 Figures of this study are available (in ASCII format) under the following link:
https://www.radar-service.eu/radar/en/dataset/tHJPPEaVtViqLpBB?token=RKDdebTwfywRJIXmPEwS.
The doi-number of the dataset is: 10.22000/1811. The context of each data file is described in detail in the header of each file.

References

Berger, U. (2008). Modeling of middle atmosphere dynamics with LIMA. *J. Atmos. Solar-Terr. Phys.*, *70*, 1170–1200. doi: 10.1016/j.jastp.2008.02.004

Berger, U., & Lübken, F.-J. (2011). Mesospheric temperature trends at mid-latitudes in summer. *Geophys. Res. Lett.*, *38*. doi: 10.1029/2011GL049528

Berger, U., & Lübken, F.-J. (2015). Trends in mesospheric ice layers in the Northern Hemisphere during 1961 - 2013. *J. Geophys. Res.*, *120*, 11,277–11,298. doi: 10.1002/2015JD023355

Berger, U., & von Zahn, U. (2002). Icy particles in the summer mesopause region: Three-dimensional modeling of their environment and two-dimensional modeling of their transport. *J. Geophys. Res.*, *107*(A11), doi:10.1029/2001JA000316.

Fiedler, J., Baumgarten, G., Berger, U., & Lübken, F.-J. (2017). Long-term variations of noctilucent clouds at ALOMAR. *J. Atmos. Solar-Terr. Phys.*, *162*, 79–89. doi: 10.1016/j.jastp.2016.08.006

Gadsden, M., & Schröder, W. (1989). *Noctilucent clouds.* New York: Springer-Verlag.

Gray, L. J., Beer, J., Geller, M., Haigh, J. D., Lockwood, M., Matthes, K., ... White, W. (2010). Solar influences on climate. *Rev. Geophys.*, *48*. doi: 10.1029/2009RG000282

Kokhanovsky, A. (2005). Microphysical and optical properties of noctilucent clouds. *Earth Sci. Rev.*, *71*, 127–146. doi: 10.1016/j.earscirev.2005.02.005

Latteck, R., Renkwitz, T., & Chau, J. L. (2021). Two decades of long-term observations of polar mesospheric echoes at 69°N. *J. Atmos. Solar-Terr. Phys.*, *216*, 105576. doi: 10.1016/j.jastp.2021.105576

Lübken, F.-J., Baumgarten, G., & Berger, U. (2021). Long term trends of mesospheric ice layers: a model study. *J. Atmos. Solar-Terr. Phys.*, 105378. doi: 10.1016/j.jastp.2020.105378

Lübken, F.-J., Berger, U., & Baumgarten, G. (2018). On the anthropogenic impact on long-term evolution of noctilucent clouds. *Geophys. Res. Lett.*, *45*, 6681–6689. doi: 10.1029/2018GL077719

Pertsev, N., Dalin, P., Perminov, V., Romejko, V., Dubietis, A., Balčiunas, R., ... Zalcik, M. (2014). Noctilucent clouds observed from the ground: sensitivity to mesospheric parameters and long-term time series. *Earth Plan. Space*, *66*(98).

Riahi, K., Rao, S., Krey, V., Cho, C., Chirkov, V., Fischer, G., ... Rafaj, P. (2011). Rcp 8.5 - a scenario of comparatively high greenhouse gas emissions. *Climatic Change*, *109*(33). doi: 10.1007/s10584-011-0149-y

Russell III, J. M., Rong, P., Hervig, M. E., Siskind, D. E., Stevens, M. H., Bailey, S. M., & Gumbel, J. (2015). Analysis of northern midlatitude noctilucent cloud occurrences using satellite data and modeling. *J. Geophys. Res.*, *119*, 3238–3250. doi: 10.1002/2013JD021017

Schmidt, F., Baumgarten, G., Berger, U., Fiedler, J., & Lübken, F.-J. (2018). Local time dependence of polar mesospheric clouds: A model study. *Atmos. Chem. Phys.*, *18*, 8893–8908. doi: 10.5194/acp-18-8893-2018

Thomas, G. E. (2003). Are noctilucent clouds harbingers of global change in the middle atmosphere? *Adv. Space Res.*, *32*, 1737–1746.

Vellalassery, A., Baumgarten, G., Grygalashvyly, M., & Lübken, F.-J. (2023). Greenhouse gas effects on the solar cycle response of water vapour and noctilucent clouds. *Ann. Geophys.*, *41*, 289–300. doi: 10.5194/angeo-41-289-2023

Warren, S. G., & Brandt, R. E. (2008, July). Optical constants of ice from the ultraviolet to the microwave: A revised compilation. *Journal of Geophysical Research: Atmospheres*, *113*(D14), 2007JD009744. Retrieved 2023-10-19, from `https://agupubs.onlinelibrary.wiley.com/doi/10.1029/2007JD009744` (775 citations (Crossref) [2023-10-19]) doi: 10.1029/2007JD009744

Yu, W., Yue, J., Garcia, R., Mlynczak, M., & Russell III, J. (2023). WACCM6 projections of polar mesospheric cloud abundance over the 21st century. *J. Geophys. Res.*, *128*(15). doi: 10.1029/2023JD038985